PNAS
www.pnas.org

Supplementary Information for

Structural basis for heme detoxification by an ABC-type efflux pump in gram-positive pathogenic bacteria

Hiro Nakamura[1, 2*], Tamao Hisano[1, 2], Md. Mahfuzur Rahman[2, 3, 4], Takehiko Tosha[2], Mikako Shirouzu[1] & Yoshitsugu Shiro[2, 3]

[1] RIKEN Center for Biosystems Dynamics Research, Yokohama, Japan

[2] RIKEN SPring-8 Center Hyogo, Japan

[3] Graduate School of Life Science, University of Hyogo, Hyogo, Japan

[4] Present address: Department of Neuroscience, University of Texas Southwestern Medical Center, Dallas, TX, USA

[*] Email: hironaka@riken.jp

This PDF file includes:

Detailed Methods

No statistical methods were used to predetermine sample size. The investigators were not blinded to the allocation during the experiments and outcome assessment.

Cloning and expression of HrtBA.

The genes encoding HrtBA subunits were amplified by PCR from *C. diphtheriae* NCTC13129 (ATCC700971D) genomic DNA, generating the *Nde*I-*Hin*dIII fragment. The *Hin*dIII site (LysLeu) that replaces the stop codon of *hrtA* enables the inframe fusion of *hrtA* and *Strep*-tag II (LysLeu*TrpSerHisProGlnPheGluLys*End). For the growth rescue experiments, the *hrtBA* DNA fragment and a synthetic DNA duplex encoding Strep-tag II were ligated to pMAL-p2G (New England Biolabs, N8068S)) at the *Nde*I and *Hin*dIII sites in the correct orientation (*SI Appendix*, Fig. S9). The resultant plasmid, pTac-Cd *hrtBA*str, expresses the *hrtBA* gene under the control of the *tac* promoter. The gene encoding the outer membrane heme receptor ChuA was amplified by PCR from the *E. coli* O157:H7 strain Sakai genomic DNA, provided by Osaka University, RIMD-PMRU, and then cloned downstream of the promoter for the ampicillin-resistance gene (P_{Ap}) in pACYC177 (1) by overlap extension PCR to replace the Ap-resistance coding region. The P_{Ap}-*chuA* DNA fragment was subcloned into pACYC184 (1) at the *Bam*HI and *Pst*I sites, generating pCm-P_{Ap}-*chuA* in which the *chuA* gene is constitutively expressed under the control of P_{Ap} (SI Appendix, Fig. S9). In growth rescue experiments, *E. coli* K12 strain JW0451(*acrB*::Km^r) (National Institute of Genetics, National BioResource Project, Japan) carrying pCm-P_{Ap}-*chuA* and pTac-Cd *hrtBA* was grown at 37°C in M63 minimal medium (100 mM K_2HPO_4/KH_2PO_4, 15 mM $(NH_4)_2SO_4$, 1 mM $MgSO_4$, 0.5% (w/v) glucose, adjusted to pH 7.0), supplemented with 0.1% LB medium (1% (w/v) tryptone, 0.5% (w/v) yeast extract, 0.5% (w/v) NaCl) and 1 μM $FeCl_3$/2 μM citric acid instead of 1.8 μM $FeSO_4$. The chloramphenicol and ampicillin concentrations were 40 μg/ml and 50 μg/ml, respectively. The medium was inoculated with frozen LB-grown glycerol stock and cultured overnight. The overnight culture was diluted 1,000-fold into the same medium, and aliquots were dispensed into culture tubes supplemented with 1/1,000 volume of heme-DMSO solutions containing various concentrations of heme. The cells were grown in the dark at 37°C for 24 h in the presence of 0.5 mM isopropyl-β-D-thiogalactoside (IPTG), and the culture tubes were photographed. Doubling times were calculated from the logarithmic growth phase using starter cultures with optical density at 650 nm of 0.02.

For protein purification, the *hrtBA*str genes were cloned into the pRSET-C vector (Thermo Fischer Scientific, V35120) to generate pT7-Cd *hrtBA*str, which produces the

intact HrtB and HrtA accompanied by a Strep-tag II at the C-terminus (*SI Appendix*, Fig. S9). The *E. coli* BL21(DE3) Star strain carrying pT7-Cd *hrtBA*str was grown overnight in 4 l of LB medium at 28°C without IPTG induction. The harvested cells were stored at -80°C.

Purification of HrtBA.

A 10 g portion of the wet cells was subjected to spheroplast formation in 30 mM Tris HCl (pH 8.0), 20% (w/v) sucrose, 10 mM EDTA, and 0.2 mg/ml lysozyme. The spheroplasts were disrupted by 2–3 passages through a French pressure cell (Ohtake Seisakusho, Tokyo) at 14,000 psi, and the membrane fractions containing ~450 mg of protein were obtained by ultracentrifugation at 168,000*g* for 90 min. The membranes were dispersed at 10 mg protein/ml in 20 mM Tris HCl (pH 8.0), 0.15 M NaCl, 1 mM EDTA, 15% (v/v) glycerol, 1% (w/v) *n*-dodecyl-β-D-maltoside (DDM; Dojindo, D316 or Anatrace, D310), and 1 mM phenylmethylsulfonyl fluoride for 30 min at 4°C with gentle stirring. The solubilized proteins were obtained by ultracentrifugation at 270,000 *g* for 30 min and applied on a *Strep*-Tactin® Superflow (IBA, 2-1208-010) column (5 ml bed volume). After washing with six column volumes of buffer containing 0.015% (w/v) *n*-dodecyl-β-D-maltoside (DDM), the HrtBA protein was eluted with 2.5 mM desthiobiotin (Iba, 2-1000-002). The concentrated eluate was purified on a Superdex 200 pg column (16/600; GE Healthcare, 28-9893-35), equilibrated with 20 mM Tris HCl (pH 8.0), 150 mM NaCl, 15% (v/v) glycerol, and 0.015% (w/v) DDM, at a flow rate of 0.75 ml/min. The concentrated peak fractions were either used for crystallization or stored for biochemical analysis at -28°C. For the crystallization of unliganded HrtBA, gel filtration column chromatography was performed at pH 7.5.

For the crystallization of AMPPNP-bound HrtBA, the eluate from the *Strep*-Tactin column was subjected to chromatography on a Superdex 200 pg column, equilibrated with 20 mM Tris HCl (pH 8.0), 150 mM NaCl, 15% (v/v) glycerol, and 0.002% (w/v) lauryl maltose neopentyl glycol (LMNG; Anatrace, NG310). To obtain crystals of heme-bound HrtBA, the HrtBA protein retained in the *Strep*-Tactin column was washed stepwise with 0.015% (w/v) DDM and 0.1% (w/v) LMNG, and then eluted with 2.5 mM desthiobiotin in the presence of 0.002% (w/v) LMNG. The protein was further purified by Superdex 200 pg column chromatography in the presence of 0.002% (w/v) LMNG at pH 8.0.

Incorporation of HrtBA into lipid nanodiscs.

A membrane scaffold protein (MSP1D1)-producing plasmid (2) was generated by

deletion of the *Sac*I-*Sac*I 198 bp DNA fragment and recircularization of pMSP1E3D1 (2) (Addgene, 20066). MSP1D1 was purified using an established protocol (2), with a slight modification as follows. Omitting DNaseI treatment, the sonicated cleared lysate was applied to a Ni-NTA Sepharose column (Qiagen, 30210). After washing the column with sodium cholate buffer, the procedures were performed in the presence of 0.02% (w/v) DDM. For nanodisc formation, MSP1D1 (216 μg), the HrtBA heterotetramer (930 μg), and *E. coli* polar lipids (400 μg) were mixed in 0.5 ml of 50 mM Tris HCl (pH 8.0), 50 mM NaCl buffer containing 0.1% (w/v) DDM to yield 20 μM, 15 μM, and ~1 mM, respectively. After gently mixing at 25°C for 0.5 h, the detergent was removed twice with 0.1 g Bio-Beads SM-2 (BIO-RAD, 1523920) at 4°C for 2 h and then once using 0.05 g Bio-Beads SM-2 at 4°C for 2 h. The nanodisc solution was subjected to ultracentrifugation at 200,000 *g* for 0.5 h to remove insoluble materials, such as proteoliposomes and aggregates. The supernatant was loaded on a Superdex 200 Increase 10/300 GL column (Cytiva, 28990944), equilibrated with 20 mM Tris HCl (pH 8.0), 100 mM NaCl, and subjected to a flow rate of 0.5 ml/min. The peak fractions were concentrated and stored at -28°C.

Measurement of ATPase activity.

The ATPase activity of HrtBA was determined using an NADH oxidation-coupled enzyme assay, as previously described (3), with slight alterations as follows. The standard reaction solution (0.4 ml) was composed of 50 mM Tris HCl (pH 8.0), 50 mM NaCl, 2 mM $MgSO_4$, 2 mM Na ATP (Sigma-Aldrich, A5394), 0.3 mM NADH (Sigma-Aldrich, N8129), 4 mM sodium phosphoenolpyruvate (Nacalai Tesque, 02852-61), 4 units of lactate dehydrogenase (Wako, 305-50951), and 4 units of pyruvate kinase (Wako, 301-50713). The pH values of the stock solutions of ATP and phosphoenolpyruvate were adjusted to 7.0 with NaOH and Tris base, respectively. The reaction was initiated by the addition of 0.8 μl of heme (Sigma-Aldrich, H9039) or protoporphyrin IX (Sigma-Aldrich, P8293) in DMSO and 4 μl of the protein (final concentration of ~2 μg/ml or 12 nM HrtBA-nanodiscs). The oxidation of NADH was monitored by measuring the absorbance at 340 nm using a DeNovix DS-11+ spectrophotometer at 37°C for 10 min, and the velocity was calculated from the linear decrease in absorbance. $MgSO_4$ was added at the same concentration as the nucleotides and the concentration of the Mg•ATP complex was calculated from a Kd of 0.014 mM (4).

Spectroscopic measurements.

The HrtBA-nanodiscs and empty nanodiscs (4 μM, 100 μl) were supplemented with 2

μM heme, in the presence or absence of nucleotides. Visible spectra were recorded at 25°C using a Shimadzu UV-2500 spectrophotometer equipped with a micro cuvette holder. Resonance Raman spectra were obtained using a single polychromator (Jovin Yvon, SPEX750M) equipped with a liquid nitrogen-cooled CCD detector (Roper Scientific, Spec 10:400B/LN). A 405 nm line from a diode laser (Ondax, SureLock LM-405-PLR-40-2) was used as the excitation line. The measurements were performed at ambient temperature using a quartz spinning cell (2,000 rpm) with an 8 mm diameter. The power of the incident excitation light was adjusted to 10 mW at the sample point. The scattered light was collected at right angles to the incident light. Calibration of the Raman lines was performed using indene. The nanodisc sample was concentrated to 24 μM containing 19 μM heme in 20 mM Tris HCl (pH 8.0) and 100 mM NaCl. Coordination and spin states were evaluated according to the assigned spectra (5).

Heme transfer assay.

The secretory heme-binding protein, HasA was produced using *E. coli* BL21 (DE3) carrying the PCR-amplified *hasADE* genes from *S. marcescens* strain CDC3100-71 ATCC® under the control of the T7 promoter in pRSET-C. The HasA protein was purified from the LB culture medium of the recombinant *E. coli* (6) with a slight modification as follows. Specifically, the $(NH_4)_2SO_4$-precipitaed proteins were dissolved in 20 mM Tris HCl (pH 8.0) and loaded on a DEAE column. HasA was eluted with a 0–0.5 M NaCl gradient in 20 mM Tris HCl (pH 8.0). The contaminating heme bound to HasA was removed by acetone/HCl treatment. The renatured protein fraction was further subjected to gel filtration column chromatography using Superdex 75 10/300 GL (GE Healthcare, 17-5174-01). HrtBA nanodiscs (4 μM) containing 2 μM heme were mixed with 4 μM HasA in the presence or absence of 2 mM ATP or AMPPNP (Sigma-Aldrich, A2647) for 5 min. The proteins (50 μl) were purified using a Superdex 200 Increase 5/150 GL (Cytiva, 28990945) in 20 mM Tris HCl (pH 8.0), 100 mM NaCl at a flow rate of 0.25 ml/min. The proteins and heme were monitored by measuring $A_{280\ nm}$ and $A_{405\ nm}$, respectively, and their contents were determined from the area of the peaks in the elution profile.

Crystallization, data collection, phase calculation, and structure refinement.

Crystallization was performed using the sitting-drop vapor-diffusion technique. For the first screening, MemGold™ HT-96 and MemGold2™ HT-96 (Molecular Dimensions, MD1-74-HT) were used with a mosquito® robot (TTP Labtech) automated system. The crystals obtained were soaked in cryoprotectant solutions in which the glycerol concentrations were gradually increased up to 20% in increments of 1%. The crystals

were then stored in liquid nitrogen. X-ray diffraction data were collected under cryogenic conditions using beamlines BL26B1/B2 (7–9), BL41XU (8, 9), and BL32XU (8–11) at SPring-8, Harima, Japan. The diffraction data were integrated and scaled using HKL2000 (12) or XDS (13) software. The structure determination procedures for the individual datasets are described below.

AMPPNP-bound HrtBA

To obtain the HrtBA-AMPPNP complex, the purified protein sample (12 mg/ml) was supplemented with 2 mM $MgCl_2$ and 2 mM AMPPNP. Crystals were grown at 4°C in drops equilibrated against 0.1 M MES (pH 6.0), 0.1 M magnesium acetate, and 22% (w/v) PEG 4000. For phase calculation by a single anomalous dispersion (SAD) analysis, the protein was complexed with 2 mM $MnCl_2$ and 2 mM AMPPNP because Mn^{2+} can substitute for Mg^{2+} in the ATPase reaction (14). Under these conditions, the crystals were grown at 4°C in drops equilibrated against 0.1 M MES (pH 6.0), 10 mM sodium acetate, 10 mM $MnCl_2$, and 22% (w/v) PEG 4000.

The crystals of HrtBA-Mg•AMPPNP and HrtBA-Mn•AMPPNP belonged to the space group $P4_22_12$, and the asymmetric unit contained each single subunit of HrtB and HrtA (a half unit of the transporter) (*SI Appendix*, Table S1). The structure of the half transporter of HrtBA-Mn•AMPPNP was solved at 3.10 Å resolution by the SAD technique, using the anomalous signal from manganese (Mn-SAD). AutoSol in Phenix (15) identified ten sites in the anomalous map, among which two major peaks were in the vicinity of the β- and γ-phosphate groups of the AMPPNP molecule bound to HrtA. One major site near the β-phosphate group is believed to correspond to the authentic Mg site for Mg• ATP in HrtA. An initial incomplete structural model of 476 residues was obtained using phenix.autobuild (15), and further model building and refinement were performed with Coot (16) and phenix.refine (15), respectively. This model was used to calculate the phases of the HrtBA-Mg•AMPPNP data.

A complete model of HrtBA-Mg•AMPPNP was constructed at a higher resolution of 2.89 Å. The HrtBA-Mg•AMPPNP model consists of 218 HrtA residues, HrtB 344 residues, one magnesium, one AMPPNP, two acetates, one glycerol, three hydrocarbon chains, and 116 water molecules. The structure of the full transporter of HrtBA-Mg•AMPPNP was obtained by generating a symmetry mate.

MnPP-bound and heme-bound HrtBA

Ligand-bound HrtBA was prepared by the addition of a 4-fold molar excess of heme or its analog, manganese protoporphyrin IX (MnPP) (Frontier Scientific, MnP562-9) to the

HrtBA eluate from gel filtration column chromatography, and the concentrated solution was used for crystallization. Red-colored crystals were grown at 20°C and 4°C in drops equilibrated against 0.1 M HEPES (pH 7.0), 0.2 M sodium acetate, 0.2 M KCl, and 22% (w/v) PEG 3000. The crystals of HrtBA containing heme or MnPP were isomorphous and belonged to the space group P1 with three heterotetramer (full transporter) molecules in the asymmetric unit (*SI Appendix*, Table S1).

Initially, MnPP-bound HrtBA was determined. Three HrtBA transporter structures, Mol1 (chains A–D), Mol2 (chains E–H), and Mol3 (chains I–L) were obtained by molecular replacement using Phaser in Phenix (15). The structures of the HrtBA-Mg•AMPPNP subunits were used as the search models. The calculated Mn-anomalous map showed two strong peaks (14.7 σ and 11.3 σ) within Mol1 and Mol2, respectively, confirming the binding of MnPP to these molecules.

After completing the structural analysis of the data of the MnPP-containing crystal, heme-containing crystals were obtained (*SI Appendix*, Fig. S10*A*). Thus, the three HrtBA structures for the data of the heme-containing crystal were determined by molecular replacement in Phaser using the structures of the MnPP-containing data. The calculated Fe-anomalous map showed two peaks (11.8 σ and 10.1 σ) for Mol1 and Mol2, respectively (*SI Appendix*, Fig. S10*B*). A square-shaped electron density was assigned to the porphyrin ring of heme, with the diagonal line of the porphyrin square aligned parallel to the molecular dyad axis of the HrtB dimer. A heme model was placed so that its propionate groups resided within the hydrophilic regions at the interface of the ECDs. Because of the lack of propionate density, there were two possibilities for the orientation of the porphyrin ring (a tilt to the front in Fig. 3*A* or to the back in Fig. 4*B*); however, both models are indistinguishable because of the pseudosymmetric environment around the heme-binding site. The structure was determined by model building and refinement in Coot and phenix.refine, respectively. The distances between the Fe atoms of heme (chains B and F) and the side chain oxygen atoms of Glu219 (chains B, D, F, and H) were restrained to 2.1 Å in the refinement. The current model consists of 216–219 residues for the six HrtA subunits, 341–343 residues for the six HrtB subunits, two heme molecules, and six lipid molecules. The individual chains of HrtA and HrtB in the three molecules are very similar, with Cα rmsd values of 0.32–0.84 Å and 0.59–1.55 Å, respectively. Furthermore, the overall structures of Mol1 and Mol2 are similar, with Cα deviation of ~1.9 Å, whereas that of Mol3 deviates because of the large difference in the HrtB dimerization mode. Because the Mol3 structure is similar to that of native HrtBA (see below), we designated it as an unliganded form.

Unliganded HrtBA

The purified HrtBA was mixed with *E. coli* polar lipids in a 1:20 molar ratio and crystallized at 20°C in drops equilibrated against 0.1 M sodium citrate (pH 6.0), 0.1 M NaCl, 0.2 M ammonium sulfate, 21% PEG 2000, 3 mM CHAPS, and 5 mM $CuCl_2$. The transparent crystals (*SI Appendix*, Fig. 10*C*) belonged to the space group $P2_12_12$ and contained each of the HrtB and HrtA subunits in the asymmetric unit (*SI Appendix*, Table S1 and Fig. S10*D*). The structure of unliganded HrtBA was obtained at 2.80 Å by molecular replacement in Phaser using the structure of Mol3 of the MnPP-containing data as a search model, followed by model building and refinement in Coot and phenix.refine, respectively. Residues 38–220 of HrtB were excluded from the model because their electron densities were not visible, probably due to their flexibility (*SI Appendix*, Fig. S10*D*). The current model consists of 221 HrtA residues, 159 HrtB residues, one sulfate, and 44 water molecules. The obtained structure is very similar to that of Mol3 from the heme-containing crystal data (Cα rmsd of 0.675 Å) (*SI Appendix*, Fig. S10*E*).

The quality of the structural models was assessed using MolProbity (17). The data and refinement statistics are summarized in *SI Appendix*, Table S1.

Amino acid sequence alignment.

The amino acid sequences of the HrtA and HrtB orthologs were retrieved. The *C. diphtheriae* (WP_010935760.1, WP_010935761.1), *S. aureus* (WP_001229911.1, WP_000761395.1), *Lactococcus lactis* (WP_011834634.1, WP_011834635.1), *Streptococcus agalactiae* (WP_001274148.1, WP_000017573.1), and *Bacillus anthracis* (WP_000202582.1, WP_000477731.1) sequences were aligned by Clustal Ω.

References cited in detailed methods

1. A. C. Chang, S. N. Cohen, Construction and characterization of amplifiable multicopy DNA cloning vehicles derived from the P15A cryptic miniplasmid. *J. Bacteriol.* **134**, 1141–1156 (1978).
2. T. K. Ritchie *et al.*, Chapter 11 - Reconstitution of membrane proteins in phospholipid bilayer nanodiscs. *Methods Enzymol*. **464**, 211–231 (2009).
3. A. Karasawa *et al.,* Physicochemical factors controlling the activity and energy coupling of an ionic strength-gated ATP-binding cassette (ABC) transporter. *J. Biol. Chem.* **288**, 29862–29871 (2013).
4. P. F. Cook, M. E. Jr. Neville, K. E. Vrana, F. T. Hartl, R. Jr. Roskoski, Adenosine cyclic 3', 5'-monophosphate dependent protein kinase: kinetic mechanism for the bovine skeletal muscle catalytic subunit. *Biochemistry* **21**, 5794–5799 (1982).

5. B. S. Lou *et al.*, Resonance Raman studies indicate a unique heme active site in prostaglandin H synthase. *Biochemistry* **39**, 12424–12434 (2000).
6. N. Izadi *et al.*, Purification and characterization of an extracellular heme-binding protein, HasA, involved in heme iron acquisition. *Biochemistry* **36**, 7050–7057 (1997).
7. G. Ueno *et al.*, RIKEN structural genomics beamlines at the SPring-8; high throughput protein crystallography with automated beamline operation. *J. Struct. Funct. Genomics* **7**, 15–22 (2006).
8. H. Murakami *et al.*, Upgrade of automated sample exchanger SPACE. *J. Appl. Crystallogr.* **45**, 234–238 (2012).
9. G. Ueno *et al.*, Beamline scheduling software: administration software for automatic operation of the RIKEN structural genomics beamlines at SPring-8. *J. Synchrotron Radiat.* **12**, 380–384 (2005).
10. K. Hirata *et al.*, Achievement of protein micro-crystallography at SPring-8 beamline BL32XU. *J. Phys. Conf. Ser.* **425**, 8–12 (2013).
11. K. Yamashita *et al.*, KAMO: towards automated data processing for microcrystals. *Acta Crystallogr. D.* **74**, 441–449 (2018).
12. Z. Otwinowski, W. Minor, Processing of X-ray diffraction data collected in oscillation mode. *Methods Enzymol*. **276**, 307–326 (1997).
13. W. Kabsch, XDS. *Acta Crystallogr. D* **66**, 125–132 (2010).
14. D. L. Stauff *et al.*, *Staphylococcus aureus* HrtA is an ATPase required for protection against heme toxicity and prevention of a transcriptional heme stress response. *J. Bacteriol.* **190**, 3588–3596 (2008).
15. P. V. Liebschner *et al.*, Macromolecular structure determination using X-rays, neutrons and electrons: recent developments in Phenix. *Acta Crystallogr. D* **75**, 861–877 (2019).
16. P. Emsley *et al.*, Features and development of Coot. *Acta Crystallogr. D* **66**, 486–501 (2010).
17. V. B. Chen *et al.*, MolProbity: all-atom structure validation for macromolecular crystallography. *Acta Crystallogr. D* **66**, 12–21 (2010).
18. C. Thomas, R. Tampé, Structural and mechanistic principles of ABC transporters. *Annu. Rev. Biochem.* **89**, 605–636 (2020).

Table S1 Data collection and refinement statistics

Data collection					
Dataset	Mg•AMPPNP	Mn•AMPPNP	MnPP	Heme	Unliganded
Beamline	SPring-8 BL26B2	SPring-8 BL26B2	SPring-8 BL32XU	SPring-8 BL26B2	SPring-8 BL26B1
Wavelength (Å)	1.00000	1.89236	1.00000	1.74000	1.35000
Space group	$P4_22_12$	$P4_22_12$	P1	P1	$P2_12_12$
Cell parameters					
a, b, c (Å)	169.0, 169.0, 94.7	169.4, 169.4, 95.1	82.0, 133.5, 159.3	82.6, 135.0, 161.0	59.8, 100.5, 192.0
α, β, γ (°)	90, 90, 90	90, 90, 90	111.6, 99.7, 94.6	112.5, 100.4, 93.8	90, 90, 90
Resolution range (Å)	50 – 2.88	50 – 2.99	50 – 2.99	50 – 3.27	50 – 2.80
(Outermost shell)	(2.93 – 2.88)	(3.04 – 2.99)	(3.17 – 2.99)	(3.47 – 3.27)	(2.85 – 2.80)
Reflections	897,604	399,387	878,625	744,127	321,610
Unique reflections	31,561	28,470	239,883	187,978	28,008
Completeness	100% (99.9%)	99.8% (99.9%)	97.2% (96.8%)	97.2% (95.6%)	95.0% (63.9%)
Redundancy	28.4 (18.3)	14.0 (9.4)	3.7 (3.8)	4.0 (1.8)	11.5 (7.5)
I/sigma	28.3 (1.0)	21.9 (1.4)	4.8 (0.4)	10.6 (0.84)	39.7 (10.8)
R_{meas}	>1	>1	0.197	0.092	0.055
$CC_{1/2}$	(0.480)	(0.540)	(0.303)	(0.526)	(0.994)
Refinement					
Phasing	MR	Mn-SAD	MR	MR	MR
Resolution range (Å)	48.4 – 2.88	48.5 – 3.10	49.3 – 3.00	48.8 – 3.40	49.6 – 2.65
Reflections	29,049	24,947	239,878	167,828	29,321
No. of atoms	4,362	3,600	25,881	25,112	4,220
R_{work}	0.221	0.220	0.266	0.255	0.219
R_{free}	0.251	0.261	0.299	0.285	0.246
RMSD bond lengths (Å)	0.008	0.009	0.008	0.003	0.011
RMSD bond angles (°)	0.896	1.140	1.005	0.452	1.460
Ramachandran plot					
favoured	96.10%	90.10%	96.03%	98.24%	95.90%
allowed	3.70%	8.80%	3.49%	1.76%	4.10%
outliers	0.20%	1.10%	0.48%	0%	0%
Average B-factor (Å^2)					
Protein	43.0	90.8	134.3	167.4	202.4
Ligands and waters	35.4	–	149.5	250.8	49.6

HrtA ATPase subunit

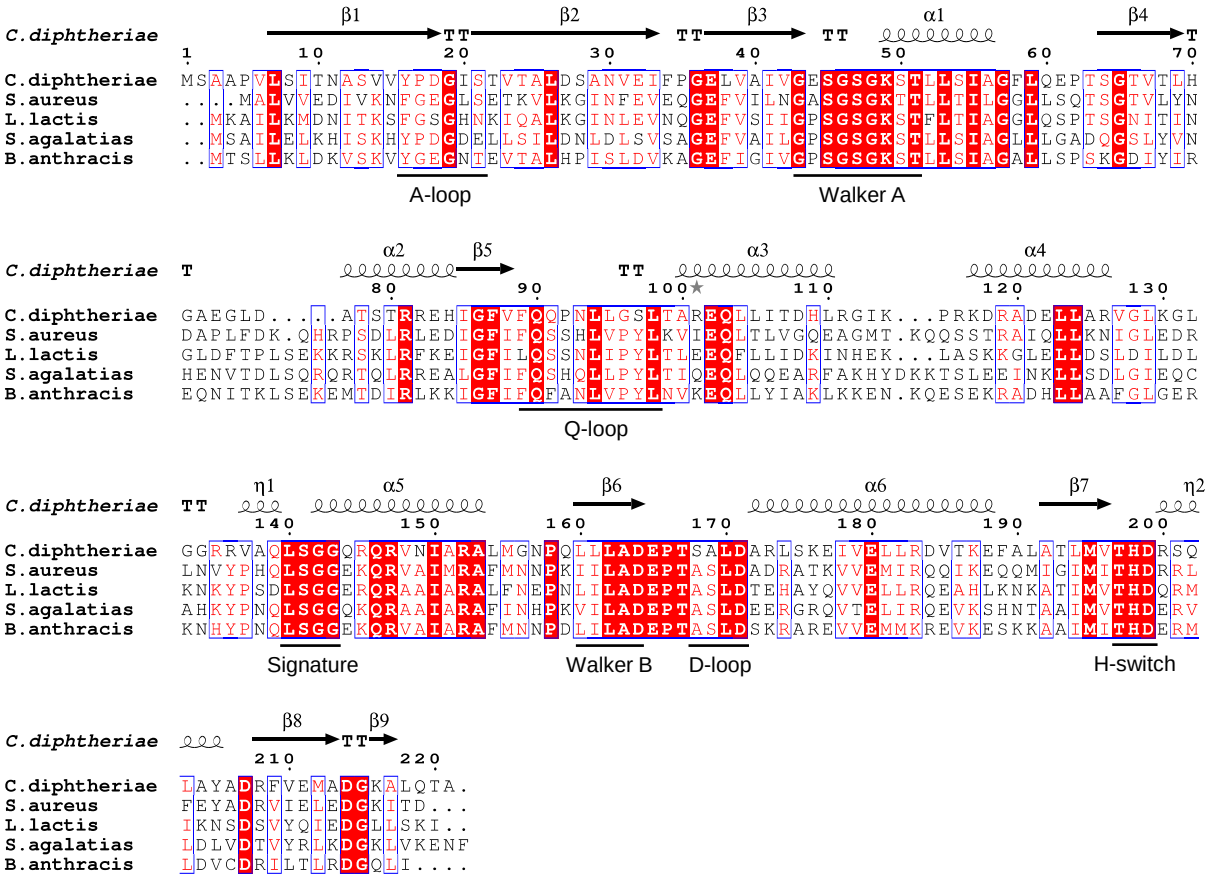

(continued)

HrtB permease subunit

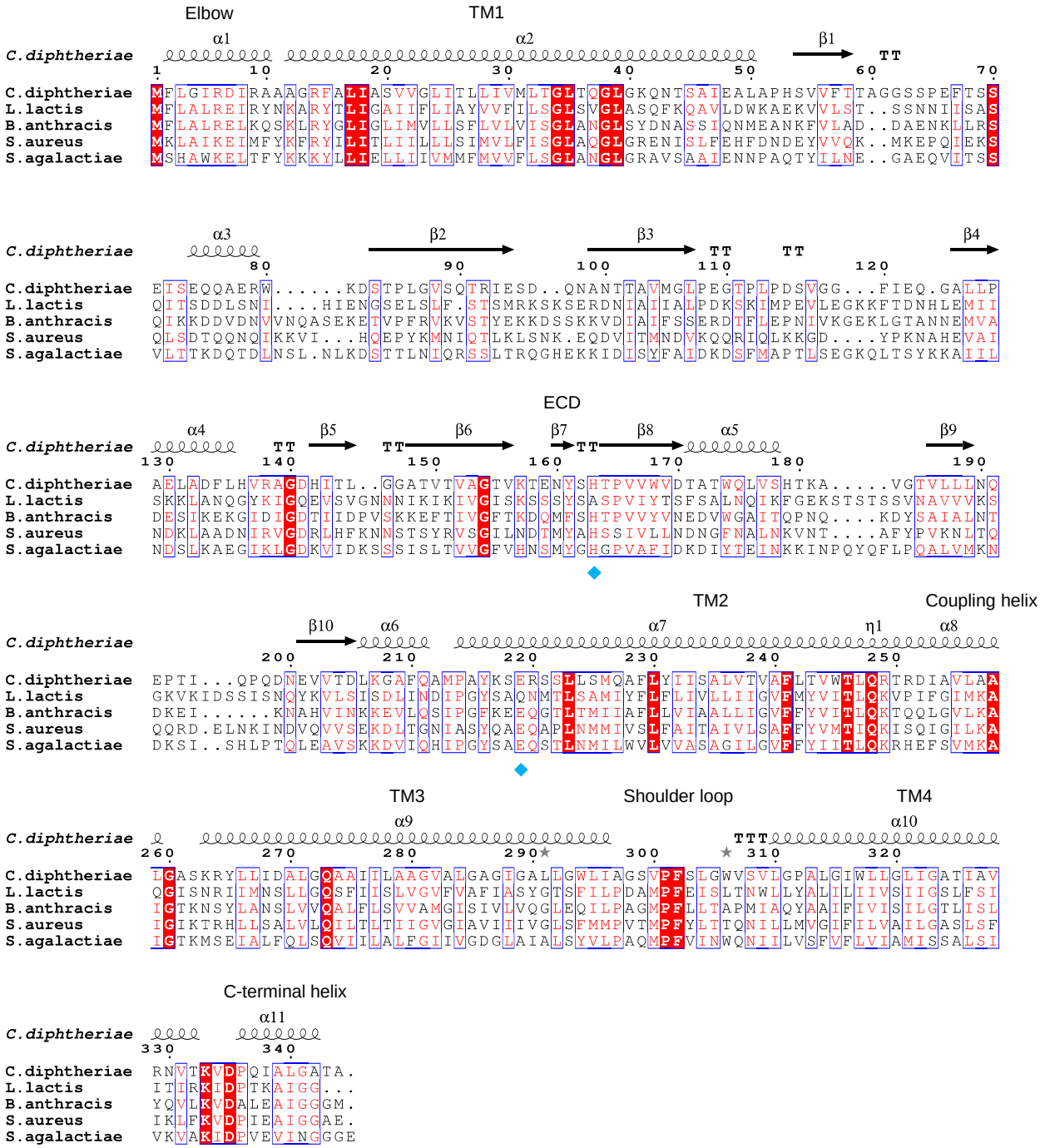

Figure S1 Alignments of amino acid sequences of HrtBA orthologs with secondary structures. The motif regions in HrtA are indicated as described previously (18). The positions of Glu219 and His163 in HrtB are indicated by sky-blue diamonds. TM, transmembrane helix; ECD, extracytoplasmic domain; α, α-helix; β, β-sheet.

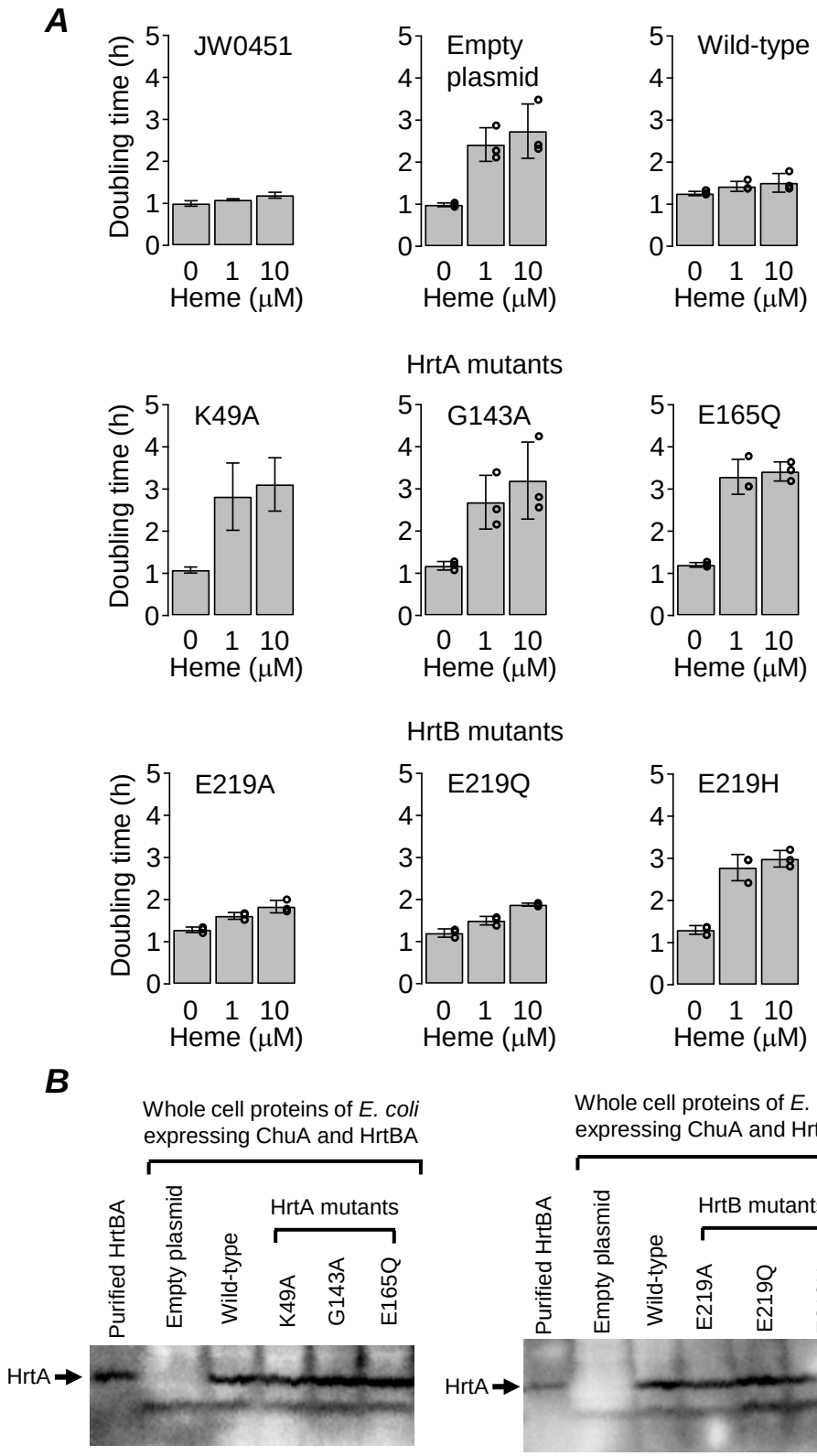

Figure S2 Growth rescue experiments in the presence of heme. (*A*) Growth doubling times of *E. coli* cells expressing wild-type HrtBA and mutants at the logarithmic growth phase. *Top*, JW0451, a parental strain; +ChuA, JW0451carrying the chuA chloramphenicol-resistant (Cm^r) plasmid and empty ampicillin-resistant (Ap^r) plasmid; Wild-type, JW0451 carrying the *chuA* Cm^r plasmid and *hrtBA* Ap^r plasmid. *Middle*, Strains carrying HrtA mutant plasmids. *Bottom*, Strains carrying HrtB mutant plasmids. n=3. (*B*) Expression of HrtA subunits. HrtA subunits were detected by western blotting using an anti-Strep tag antibody conjugated with horse radish peroxidase (HRP). HRP signals were visualized by the chemiluminescence imaging system, FUSION FX (Vilber). Whole cell proteins (20μg) and purified HrtBA (80 ng) were applied to an SDS-PAGE gel.

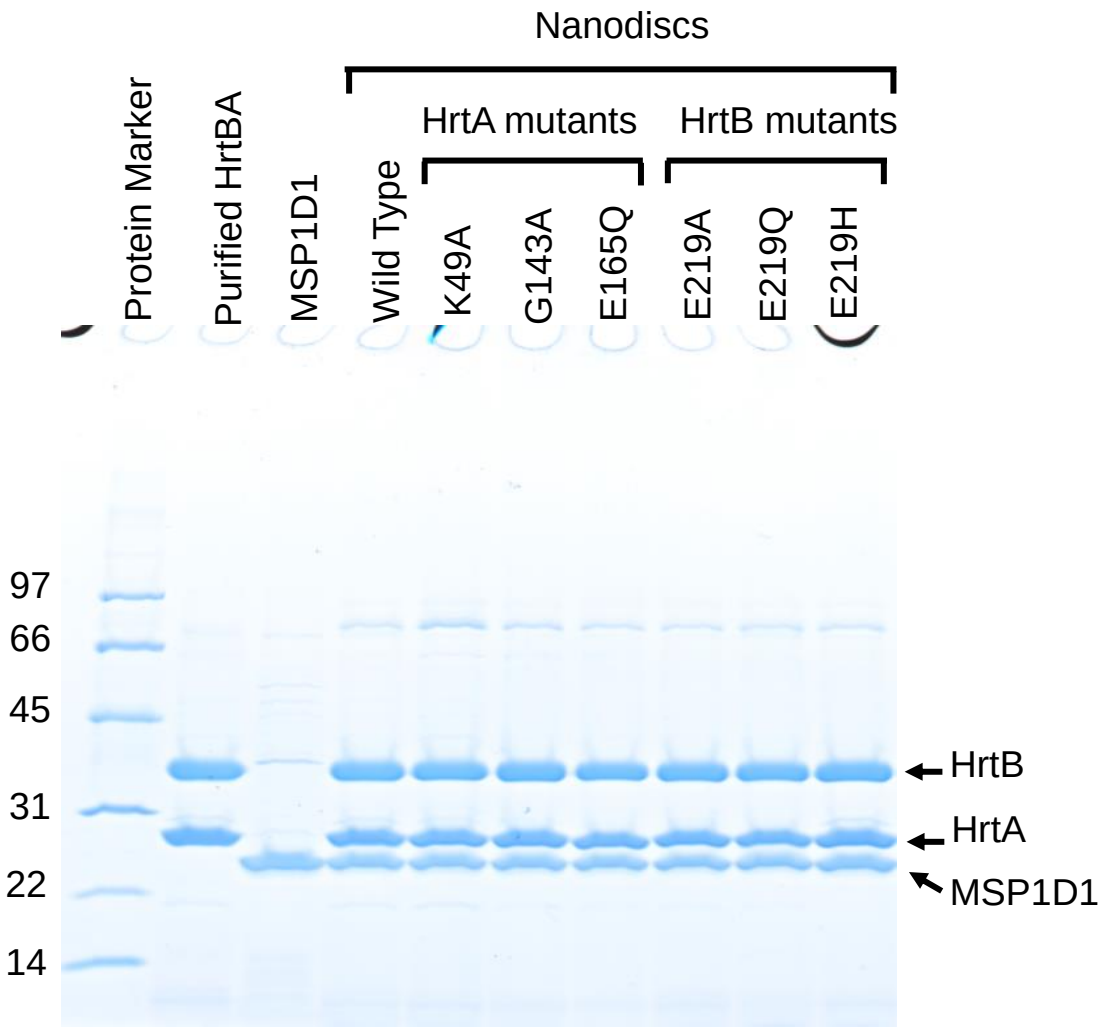

Figure S3 Coomassie brilliant blue staining of purified and nanodisc-reconstituted HrtBA on an SDS-PAGE gel. Purified HrtBA (3 μg), MSP1D1 (1 μg), and nanodisc-HrtBA and mutants (4 μg) were applied to the gel.

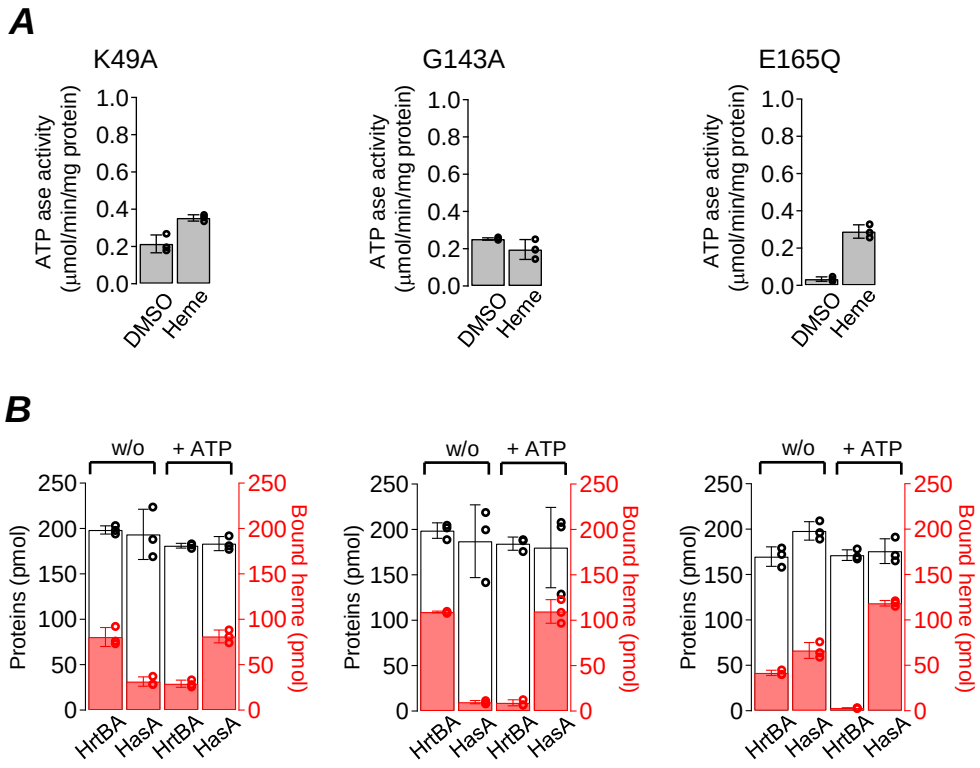

Figure S4 Functional analyses of the HrtA NBD mutants.
(*A*) ATPase activities of the mutants. (*B*) Heme transfer of the mutants. Conditions are described in the legend of Fig. 1.

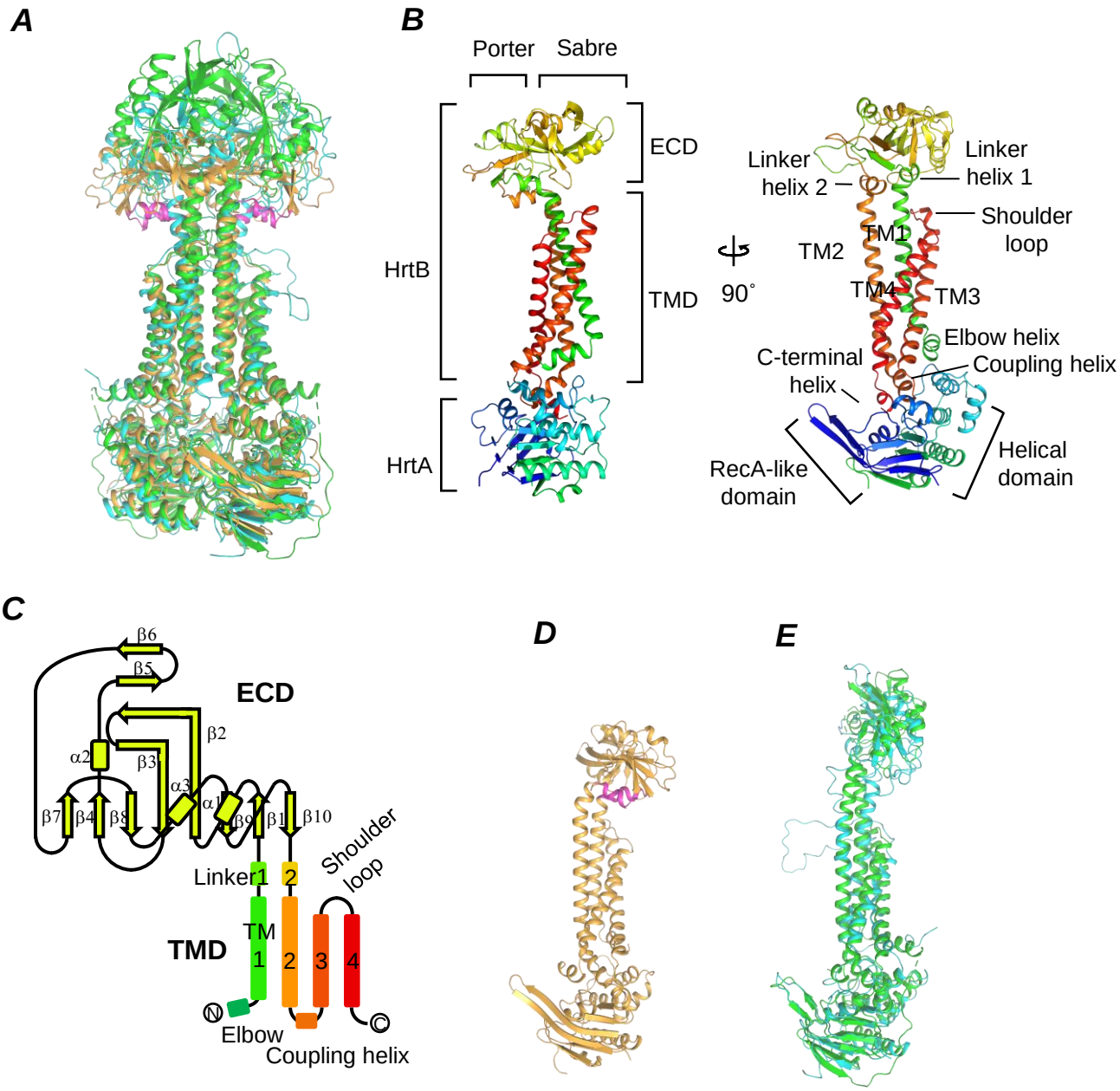

Figure S5 Structure of HrtB and HrtA. (*A*) Overall structure of HrtBA, MacB, and LolCDE. Superimposition of nucleotide-bound forms of HrtBA (orange), MacB (green; PDB ID, 5LIL), and LolCDE (cyan; PDB ID, 7ARK). Linker helices in HrtBA are colored in magenta. (*B*) Structural dissection of HrtB and HrtA into their subdomains. (*C*) Secondary structure of HrtB. (*D*) HrtBA. (*E*) Superimposition of MacB (green) and LolDE (cyan). (*F*) Unliganded HrtBA. (*G*) Unliganded MacB (PDB ID, 5WS4). ECD, extracytoplasmic domain; TMD, transmembrane domain; TM, transmembrane helix; α, α-helix; β, β-sheet.

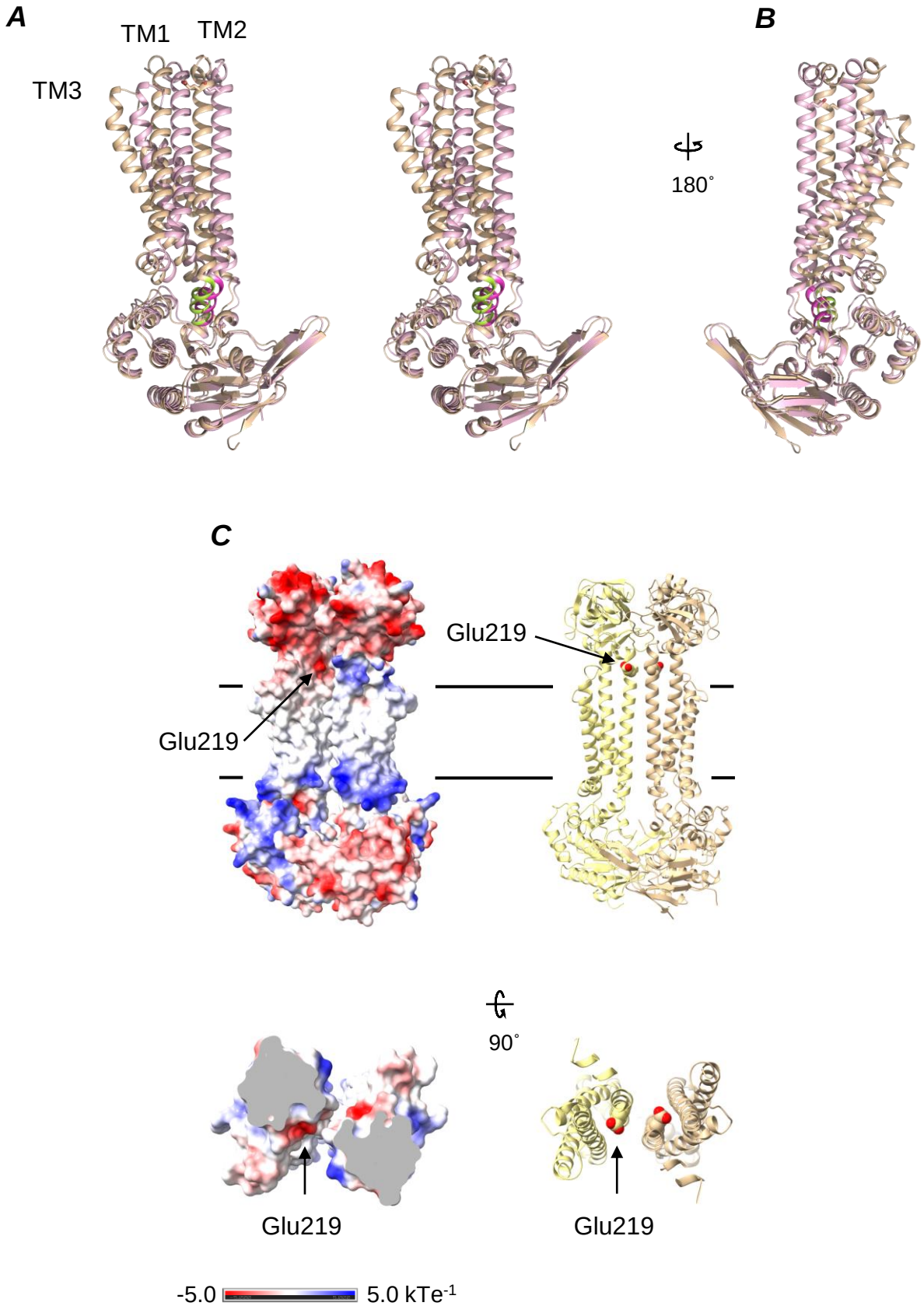

Figure S6 Structural transition from the unliganded state to the heme-bound state. (*A*) Stereo view of superimposition of the unliganded (wheat) and heme-bound (pink) states. The coupling helices are indicated in limon and magenta, respectively. (*B*) 180˚ rotation view of *A*. (*C*) Electrostatic surface of the unliganded HrtBA generated by Chimera X (13). Negative and positive regions are indicated by red and blue gradients, respectively (*left*). Same view of the unliganded structure of HrtBA (*right*). Glu219 is indicated as a sphere. TM, transmembrane helix.

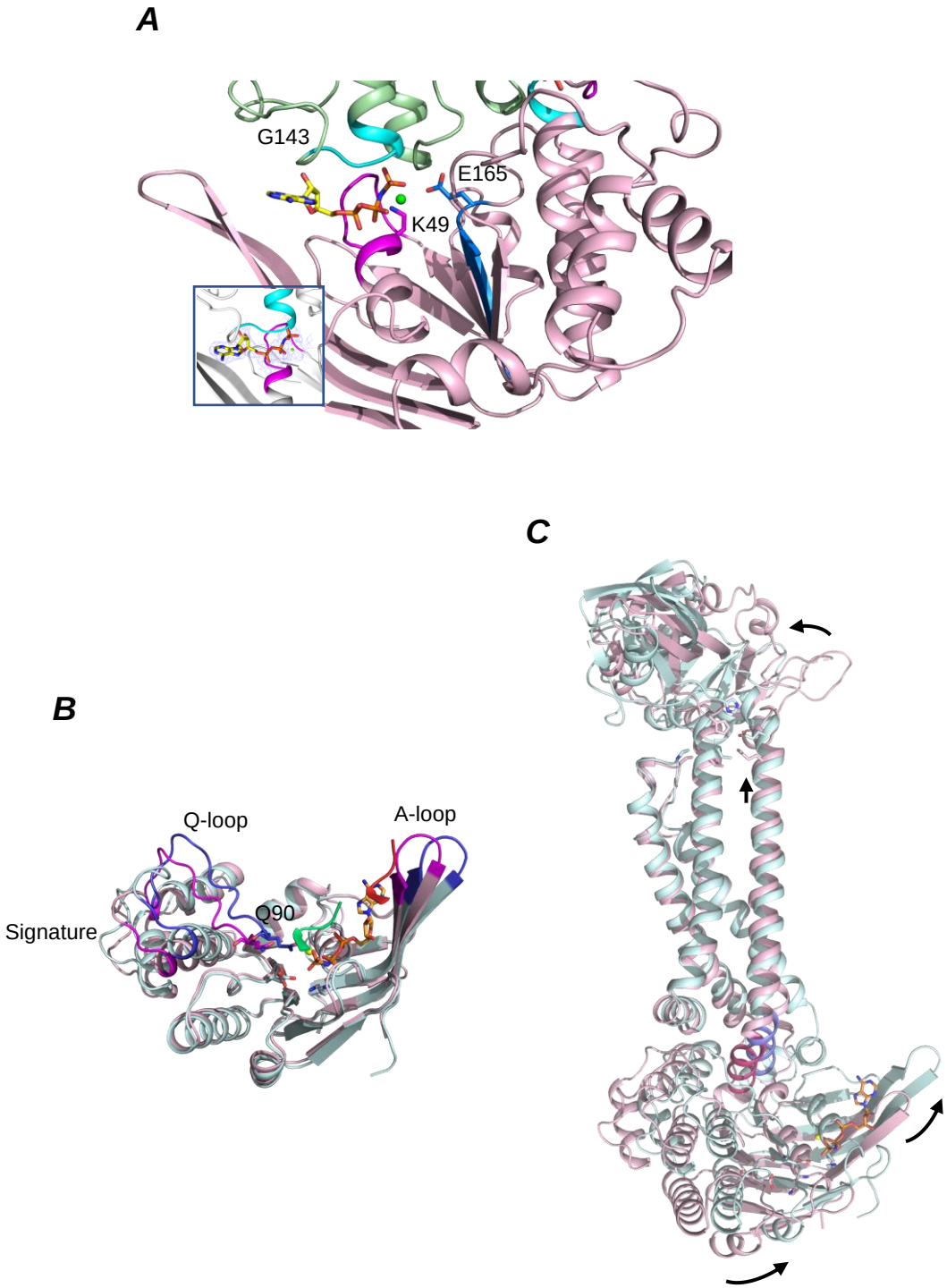

Figure S7 Structure of AMPPNP-bound HrtA and transition from heme-bound HrtBA to AMPPNP-bound state. (*A*) Structure of AMPPNP-bound HrtA. AMPPNP and Mg are depicted using stick models and a green ball, respectively. The Walker A, Walker B, and signature regions are indicated in magenta, blue, and cyan, respectively. *Inset* 2Fo-Fc electron density map for bound AMPPNP, contoured at 1.5 σ. (*B*) Induced fit of the NBD upon nucleotide binding from the heme-bound state (pink) to the AMPPNP-bound state (cyan). Truncated signature regions of the opposite subunit are colored in red (heme-bound) and turquoise (AMPPNP-bound). (*C*) Conformational change in the TMD induced by nucleotide binding in the NBD. Coupling helices in the heme-bound and AMPPNP-bound states are colored magenta and blue, respectively.

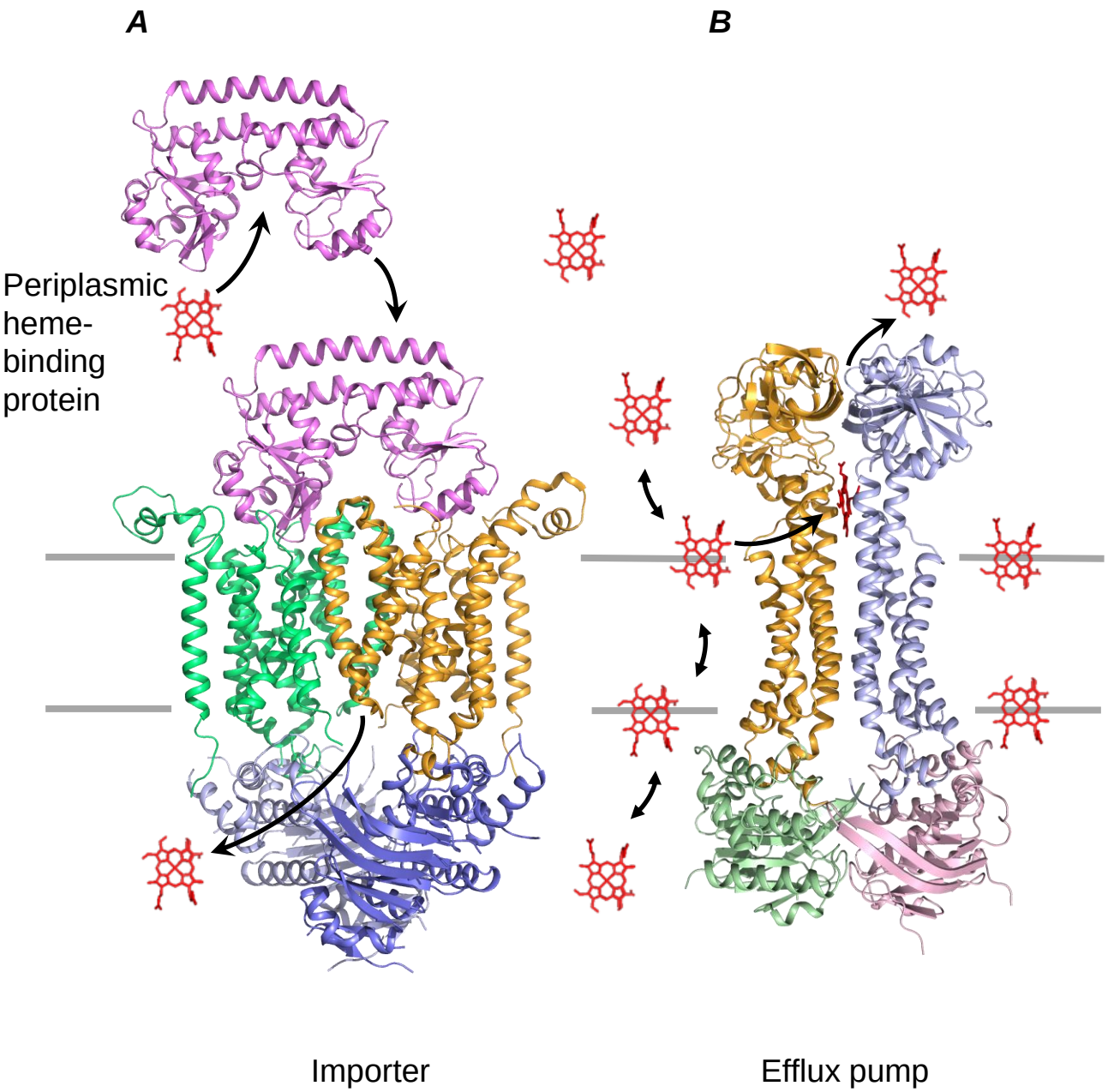

Figure S8 Bacterial ABC-type heme importer *versus* heme efflux pump. (*A*) Bacterial heme importer complex (the heme-free complex, PDB ID, 5B58). In the heme acquisition system, the host heme acquired is relayed from heme-binding proteins to the cognate ABC importer complex, and the internalized heme is sequestered again by apo-hemoproteins or heme oxygenase. The binding proteins use His and Tyr as heme ligands. The heme-binding proteins localized in the peptidoglycan layers were omitted. (*B*) HrtBA (heme-bound form).

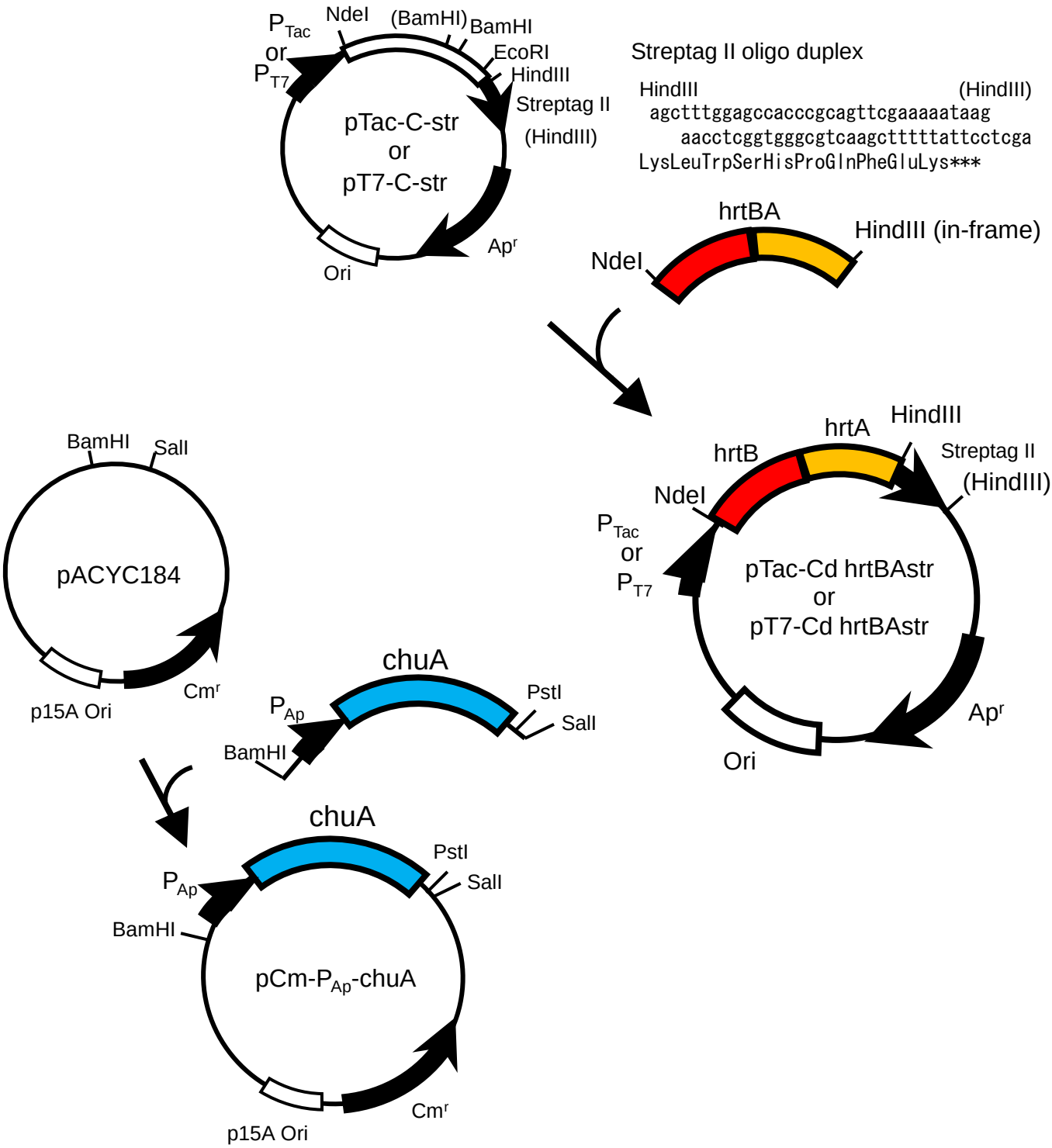

Figure S9 Plasmid construction of pTac-Cd hrtBA, pT7-Cd hrtBAstr, and pCm-P_{Ap}-chuA. Details are provided in the *SI Appendix*, Detailed Methods section.

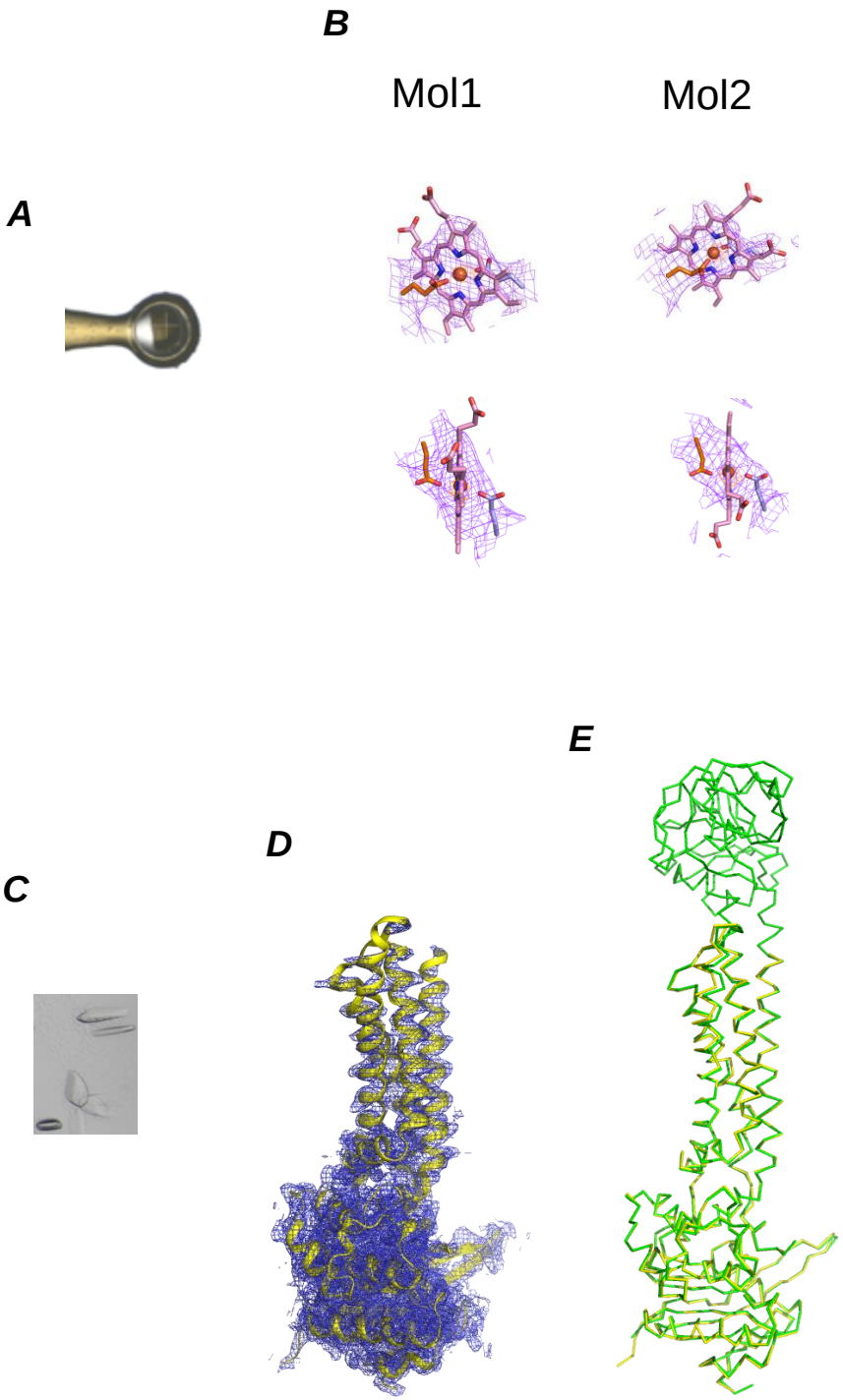

Figure S10 Crystal structures from unliganded and heme-bound HrtBA preparations. (*A*) A crystal from the heme-bound HrtBA preparation. (*B*) Omit maps for the bound heme and Glu219 contoured at 1.0 σ (pink) and Fe anomalous peaks contoured at 9.5 σ and 8.0 σ (orange) in Mol1 and Mol2, respectively. (*C*) Crystals of unliganded HrtBA. (*D*) Electron density for the unliganded HrtBA data (contoured at 1.0 σ), overlaid with the structural model. (*E*) Superimposition of the structures of unliganded HrtBA (yellow) and Mol3 from the heme-bound crystal data (green).